FINAL REPORT

Micro Ion Mobility Sensor for In Situ Monitoring of Contaminated Groundwater

SERDP Project ER-1603

January 2012

Jun Xu
Oak Ridge National Laboratory

This document has been cleared for public release

SERDP
DOD ▪ EPA ▪ DOE

This report was prepared under contract to the Department of Defense Strategic Environmental Research and Development Program (SERDP). The publication of this report does not indicate endorsement by the Department of Defense, nor should the contents be construed as reflecting the official policy or position of the Department of Defense. Reference herein to any specific commercial product, process, or service by trade name, trademark, manufacturer, or otherwise, does not necessarily constitute or imply its endorsement, recommendation, or favoring by the Department of Defense.

REPORT DOCUMENTATION PAGE

Form Approved
OMB No. 0704-0188

The public reporting burden for this collection of information is estimated to average 1 hour per response, including the time for reviewing instructions, searching existing data sources, gathering and maintaining the data needed, and completing and reviewing the collection of information. Send comments regarding this burden estimate or any other aspect of this collection of information, including suggestions for reducing the burden, to the Department of Defense, Executive Services and Communications Directorate (0704-0188). Respondents should be aware that notwithstanding any other provision of law, no person shall be subject to any penalty for failing to comply with a collection of information if it does not display a currently valid OMB control number.
PLEASE DO NOT RETURN YOUR FORM TO THE ABOVE ORGANIZATION.

1. REPORT DATE *(DD-MM-YYYY)*	2. REPORT TYPE	3. DATES COVERED *(From - To)*
01-2012	Final Report	01-2008-01-2012

4. TITLE AND SUBTITLE
Micro Ion Mobility Sensor for In Situ Monitoring of Contaminated Groundwater

5a. CONTRACT NUMBER

5b. GRANT NUMBER

5c. PROGRAM ELEMENT NUMBER

6. AUTHOR(S)
Jun Xu

5d. PROJECT NUMBER
ER-1603

5e. TASK NUMBER

5f. WORK UNIT NUMBER

7. PERFORMING ORGANIZATION NAME(S) AND ADDRESS(ES)
Oak Ridge National Laboratory
P.O. Box 2008, MS 6201
Oak Ridge, Tennessee 37831

8. PERFORMING ORGANIZATION REPORT NUMBER

9. SPONSORING/MONITORING AGENCY NAME(S) AND ADDRESS(ES)
SERDP/ESTCP
4800 Mark Center Drive, Suite 17D08
Alexandria, VA 22350-6386

10. SPONSOR/MONITOR'S ACRONYM(S)
SERDP/ESTCP

11. SPONSOR/MONITOR'S REPORT NUMBER(S)
ER-1603

12. DISTRIBUTION/AVAILABILITY STATEMENT
Unlimited

13. SUPPLEMENTARY NOTES

14. ABSTRACT
The objective of this project, was therefore, to develop a prototype sensor technology, membrane-extraction (ME)-IMS, that could be used in situ or ex situ, to characterize the extent of groundwater plumes, conduct compliance monitoring around waste facilities or at the leading edge of a plume, and monitor remedial actions. The IMS instrument could also be used to monitor CHC in the vapor phase.

15. SUBJECT TERMS

16. SECURITY CLASSIFICATION OF:			17. LIMITATION OF ABSTRACT	18. NUMBER OF PAGES	19a. NAME OF RESPONSIBLE PERSON
a. REPORT	b. ABSTRACT	c. THIS PAGE		42	Ronald W. Falta
					19b. TELEPHONE NUMBER *(Include area code)* 865-574-8955

Reset

Standard Form 298 (Rev. 8/98)
Prescribed by ANSI Std. Z39.18

FINAL REPORT
Project: ER-1603

TABLE OF CONTENTS

Page

1.0 EXECUTIVE SUMMARY 1
- 1.1 OBJECTIVES 1
- 1.2 TECHNICAL APPROACH 1
- 1.3 RESULTS 1
- 1.4 BENEFITS 2

2.0 OBJECTIVE 3

3.0 BACKGROUND 4
- 3.1 MEMBRANE EXTRACTION 4
- 3.2 ION MOBILITY SPECTROMETRY 6
- 3.3 GC/DMS ANALYZER 9

4.0 MATERIALS AND METHODS 11
- 4.1 IDENTIFICATION BY ME-IMS 11
- 4.2 IDENTIFICATION BY ME-GC/DMS 12
- 4.3 INTERFERENCE TEST 14
- 4.4 SENSITIVITY TEST 16
- 4.5 DYNAMIC RANGE AND CALIBRATION CURVES 17

5.0 RESULTS AND DISCUSSION 20
- 5.1 CONTAMINANT IDENTIFICATION 21
  - 5.1.1 06-11 MW 21
  - 5.1.2 06-12 MW 21
- 5.2 CONTAMINANT QUANTIFICATION 22
- 5.3 DEPTH MONITORING 23

6.0 CONCLUSIONS AND IMPLICATIONS FOR FUTURE RESEARCH 25
- 6.1 CONCLUSIONS 25
- 6.2 IMPLICATIONS FOR FUTURE RESEARCH 26

7.0 LITERATURE CITED 28

APPENDIX A MODELING A-1
APPENDIX B PUBLICATIONS, PATENTS, AWARD B-1

LIST OF FIGURES

Page

Figure 1. Illustration of envisioned in situ unintended monitor powered by solar cells and transmitted via wireless, for monitoring CHCs in groundwater. Elements of ME-IMS technology. 4
Figure 2. Illustration of membrane loop for converting chlorinated solvents into vapor phase. 5
Figure 3. Illustration of membrane sampling system capable of multi-functional extraction of CHCs from water. 6
Figure 4. Images of multi-loop membrane extraction device. 6
Figure 5. Inner elements of IMS-DMS analyzer, outer interface of IMS-DMS analyzers, and B-N gate. 7
Figure 6. Photos of the atmosphere pressure ionization and reaction chamber. One of 14 electrodes. 8
Figure 7. Parts and assembly of IMS-DMS interface. 8
Figure 8. Sionex DMS filtration chip (Mosley, 2010). 10
Figure 9. IMS spectrum for dry air flowing into a 50 cm PDMS membrane tube. 11
Figure 10. Negative mode IMS spectra for TCE, PCE, and CH_3I, spiked in water with concentrations of 10 ppm respectively (Du et al., 2010). 12
Figure 11. 2D GC/DMS spectra of 435µg/L TCE (300 ppbv) and 490µg/L PCE in water both in positive mode and negative mode. 13
Figure 12. Detection of *trans*-1,2-DCE with IMS (saturated headspace vapor) and membrane GC/ DMS system (200 ppbv). 14
Figure 13. Separation of eight VOC mixed in water: PCE, Toluene, TCE, Benzene, CH_2Br_2, CCl_4, $CHCl_3$, and *trans*-1,2-DCE. 14
Figure 14. 2D plots from the ME GC DMS analysis of the mixture of 28 chemicals in water. 16
Figure 15. LODs for TCE as a function of sampling time (5 ppbv, negative ions). 17
Figure 16. TCE tailing and cracking effects in negative mode and corresponding positive mode signals. 18
Figure 17. TCE signal intensity as a function of concentration. 18
Figure 18. Photos of field testing in NASA SSC. 20
Figure 19. 2D Spectra depicting TCE contamination detected by membrane GC/DMS in specific ion mode. 21
Figure 20. 2D spectra of contaminants in 06-12 MW for negative and positive mode. 22
Figure 21. Planar view of 2D spectra. 22
Figure 22. Distribution of TCE concentration as a function of depth for MW 06-11 well measured by the membrane GC/DMS monitor. 24

LIST OF TABLES

Page

Table 1. System parameters used in our experiments. 13
Table 2. Identification parameters for different chemicals with GC/DMS..... 15
Table 3. TCE concentrations and ID parameters for MW 06-11 and MW 06-12 wells. 23

ACRONYMS AND ABBREVIATIONS

2D	two-dimensional
APCI	atmosphere-pressure chemical ionization
B-N	Bradbury-Nielson
CHC	chlorinated hydrocarbon
DCE	dichloroethylene
DF	dilution flow
DMS	differential mobility spectrometry
DNAPL	dense non-aqueous phase liquid
E	electric field
GC	gas chromatography or
GC/DMS	gas chromatographic differential mobility spectrometry
ID	inside diameter
IMS	ion mobility spectrometry
K	mobility coefficient
kHz	kilohertz
kV	kilovolts
LOD	limit of detection
LTM	long-term monitoring
MΩ	Megaohm
μg/L	microgram per liter
m/Z	mass-to-charge
ME	membrane-extraction
ME-GC/DMS	membrane-extraction gas chromatographic differential mobility spectrometry
ME-IMS	membrane-extraction ion-mobility spectrometry
MHz	megahertz
MS	mass spectrometry
MW	monitoring well
N	density of neutral drift molecules
NASA	National Aeronautics and Space Administration

ACRONYMS AND ABBREVIATIONS (continued)

OD	outside diameter
ORNL	Oak Ridge National Laboratory
PCB	printed circuit board
PCE	tetrachloroethylene
PDMS	polydimethylsiloxane
ppb	part per billion
ppbv	parts per billion by volume
ppm	parts per million
ppmv	parts per million by volume
PTFE	polytetrafluoroethylene
RF	radio frequency
RIP	reactant ion peak
s	second
S/N	signal-to-noise ratio
SCCM	standard cubic centimeters per minute
SERDP	Strategic Environmental Research and Development Program
SSC	Stennis Space Center
TCE	trichloroethylene
T_r	retention time
USEPA	U.S. Environmental Protection Agency
V/A	volts per ampere
V/cm	volts per centimeter
V_C	voltage compensation
V_d	drift velocity
VOC	volatile organic compounds

ACKNOWLEDGEMENTS

Research was sponsored by the Strategic Environmental Research and Development Program (SERDP). Oak Ridge National Laboratory (ORNL) is managed by UT-Battelle, LLC for the U.S. Department of Energy under Contract DE-AC05-00OR22725.

Technical material contained in this report has been approved for public release.
Mention of trade names or commercial products in this report is for informational purposes only; no endorsement or recommendation is implied.

1.0 EXECUTIVE SUMMARY

1.1 OBJECTIVES

Contaminated groundwater and its associated vapor are a major concern due to the persistence of certain pollutants such as dense non-aqueous phase liquids (DNAPL). Chlorinated hydrocarbons (CHC) are particularly important because they constitute the major portion of DNAPLs. Although the government proceeds with remediation at contaminated sites, long-term monitoring (LTM) of these pollutants is needed not only because of their potential hazard, but also due to the reality that complete cleanup of significant DNAPL source zones has not and will not be possible.

Currently, most LTM approaches are relatively conventional, usually involving the installation and maintenance of monitoring wells (MW), labor intensive sampling, and costly laboratory analysis. The emergence of sensitive, robust, and fast-responding ion mobility spectrometry (IMS) technology provides the opportunity to develop an *in situ* LTM instrument with the ability to detect, identify, and quantify CHC in groundwater and soil vapors.

The objective of this project, was therefore, to develop a prototype sensor technology, membrane-extraction (ME)-IMS, that could be used *in situ* or *ex situ*, to characterize the extent of groundwater plumes, conduct compliance monitoring around waste facilities or at the leading edge of a plume, and monitor remedial actions. The IMS instrument could also be used to monitor CHC in the vapor phase.

1.2 TECHNICAL APPROACH

To achieve high reliability and low cost, three main tasks were undertaken in this project: (1) convert contaminants from liquid phase into vapor phase using a novel membrane separation; (2) achieve sensitive identification of contaminants by combining linear and nonlinear IMS; and (3) reduce costs for long-term monitoring by making the sensor operation unattended and on-site, by adapting miniaturized structures, and by avoiding the use of vacuum equipment.

A preliminary field test was conducted at National Aeronautics and Space Administration (NASA) Stennis Space Center (SSC) for the membrane extraction ion-mobility groundwater monitor. Two wells, including one with low trichloroethylene (TCE) concentration/slow recharge rate and one with high TCE concentration/fast recharge rate were tested with various water depths and timings. The monitor demonstrates a clear identification of CHC in the wells and reasonably accurate quantification. This qualitative and quantitative capability validates the proof-of-principle prototype for simultaneous sampling and analysis in a single-step within a compact in-situ and stand-alone monitor. This field test also reveals some problems that were associated with current prototype stage of the monitor, practical un-predicted environments, or in-experience in field test.

1.3 RESULTS

Lab testing showed that a prototype sensor is capable of uniquely identifying 32 volatile organic compounds (VOC), including the most common, TCE and tetrachloroethylene (PCE). Limit of

detection (LOD) for TCE is 0.37 parts per billion by volume (ppbv); well below regulatory limits.

Based on the current stage of this technology, the following key findings are summarized:

1. *Identification is reliable*. No interference from presence of other containments was observed. Only minor revision, such as simultaneous measurements of reactant-ion and sample ion peaks, is needed to achieve identification stability in field.
2. *Quantification is excellent in laboratory, but not highly accurate in field under current conditions.* From laboratory experiments, the LOD can be as low as 0.37 ppbv for TCE. Similar order for other chlorinated solvents. The monitor is very reliable for quantification at least in laboratory. However, quantification was affected by both groundwater temperature and pressure in field testing experiments. The monitor should be modified to address analysis of samples under variation of environmental conditions, such as water temperature and pressure.
3. *ME-gas chromatographic (GC) differential mobility spectrometry (DMS) (ME-GC/DMS) monitor may need to work with non-linear quantification curves.* Since these curves are stable and reproducible, the non-linear curves should be effective for calibration.
4. *Dynamic range is limited.* Current dynamic range for TCE detection is 0.5-2000 ppbv. In many groundwater wells, such as those in NASA SSC, TCE concentration is higher than 2000 ppbv. A dilution mechanism will be made so that the monitor can deal with high concentrations larger than 2 parts per million (ppm).
5. *Sensor Dimensions.* Sensor configuration and dimensions should be made more flexible to enable placement under different field scenarios (e.g., 2-inch diameter groundwater wells).”

1.4 BENEFITS

The membrane-extraction ion-mobility spectrometry (ME-IMS) technology may eliminate the need for collecting and shipping samples, and expensive offsite lab analysis, thereby reducing the cost of monitoring CHC in groundwater.

2.0 OBJECTIVE

The ultimate goal of this project was to provide unattended, analytical capabilities for on-site monitoring of chemical contaminants in groundwater. We sought to build a technology which is comparatively inexpensive and compact while achieving highly sensitive analytical performance.

The key element for achieving this goal was to combine membrane extraction with miniature linear and nonlinear IMS analyzers. The instrument directly samples groundwater and transports analytes into the analyzer. Monitoring of CHC was the focus of this project.

Specific objectives included:

1. Build a linear and nonlinear IMS for two-dimensional (2D) separation of CHC.
2. Use both positive and negative ion detection for achieving high on-site sensitivity in less than 1 part per billion (ppb). Detection of positive ions has been used to detect high concentrations of CHC, while detection of the negative ions has been used to quantity low concentrations of the contaminants.
3. Miniaturize ionization source, IMS drift cell, and nonlinear IMS transport gap while maintaining reliability. The dimensions of the sensor were configured to be capable of in situ charactering the groundwater of 10.2-cm (4-inch) diameter wells.
4. Use membrane technology for effective conversion of contaminants from water to gaseous phase that seamlessly feeds the IMS analysis.
5. Reduce cost by making the sensor capable of on-site monitoring and unattended operation, eliminating vacuum pumps, low-power consumption, and making the sensor compatible with currently existing groundwater wells.

3.0 BACKGROUND

A prototype monitor for real-time monitoring of CHC in groundwater has been developed. The monitor is based on ME-IMS technology that is capable of combining real-time sampling with CHC extraction and detection. The monitor is a compact device capable of detecting most aqueous CHC, PCE, TCE, and dichloroethylene (DCE), with high reliability and sensitivity. Figure 1 shows basic elements of this technology, which consists of a membrane assembly, preconcentrator, and the combination of a GC-DMS analyzer and IMS analyzer. Reliability is achieved by the 2D separation, consisting of DMS compensation voltage and GC retention time.

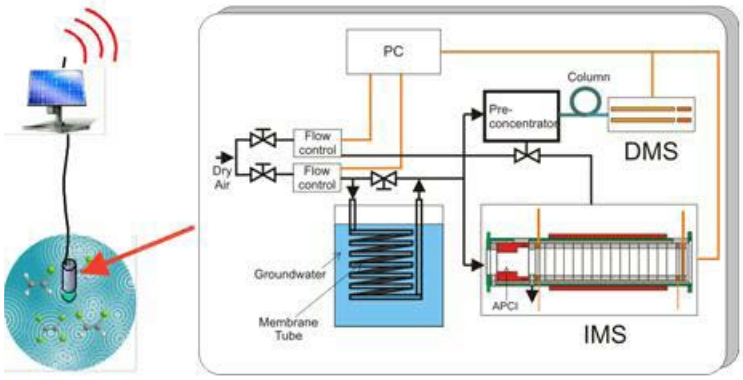

Figure 1. Illustration of envisioned in situ unintended monitor powered by solar cells and transmitted via wireless, for monitoring CHCs in groundwater (left). Elements of ME-IMS technology (right).

3.1 MEMBRANE EXTRACTION

A *membrane inlet* system will be used as a method to convert analytes presented in the liquid to a stream of carrier gas for subsequent mobility analysis. For enhanced sensitivity, this process will be carried out in two steps. In the first step, the analyte molecules are extracted into the carrier gas through the barrier membrane. In the second step, the analytes will be concentrated by a preconcentrator that can be pulse heated.

The basic membrane inlet system consists of polymeric membrane tubes immersed in water containing the analytes. Carrier gas flows through the tubes. Analytes partition between the water and the membrane layer according to Henry's law (Almquist and Hwangb, 1999). Analytes permeate to the polymer/air interface where they are volatilized by the flowing carrier gas. The process is effective because the enrichment of the polymer to volatile organics is many orders of magnitude higher than for air or water (Yeoman, et al., 2002; Ohshima, et al., 2005). Many membranes can be operated in parallel, each with selected functionality that gives high permeability for selected species. Figure 2 shows one example of spiral membranes indicated in the front end of the sensor outlined in Figure 1. These spiral membranes provide two functions, first to increase permeation rates and second to use different selective membranes to obtain multiple chemical vapors from the liquid. The objective of this work is to obtain a system capable of extracting CHC at a sufficient rate in the air flow.

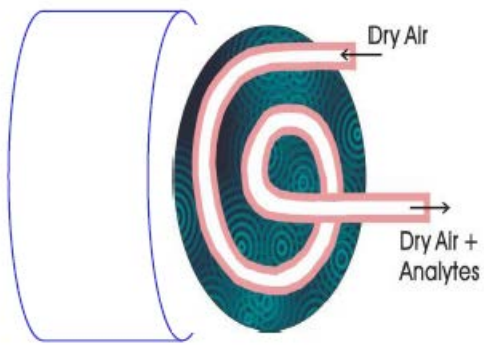

Figure 2. Illustration of membrane loop for converting chlorinated solvents into vapor phase.

Polydimethylsiloxane (PDMS) membrane tubes were commercially obtained (VWR Labshop, 20” length, 0.058” inside diameter [ID]×0.076” outside diameter [OD]×0.009” layer thickness) and used for converting chlorinated solvents from water to vapor. PDMS tubes were chosen because they are highly permeable towards organic vapor and show good chemical stability. The tube ID was 1.47 mm and the wall thickness was 0.23 mm. The length of the membrane that was in direct contact with water varied from 8 cm to 150 cm. Since the as-received membrane was typically contaminated with solvents and impurities, these membranes were cleaned initially in a methanol bath followed by a methanol removal procedure. Then the membrane was further cleaned by flushing the inside of the membrane tube with dry air and annealing in hot water. This procedure took about 20 hours. The entire cleaning procedure was monitored using an on-line miniature ion mobility spectrometer. The permeation temperature was controlled in the range of 0-70 °C using a magnetic stirrer heater (CAT, MCS67).

A multi loop functional membrane sampling system was constructed for effective extraction of CHC from water. Figure 3 illustrates the membrane sampling system capable of multi-functional extraction of CHC from water. This membrane system includes 8 elements: (1) carrier-gas inlet, (2) carrier-gas distributor, (3) water-loop, (4) water-to-vapor chamber, (5) permanent collector, (6) second-stage carrier gas inlet, (7) vapor-to-vapor chamber, (8) permanent analyte outlet. The assembly details of this multi-loop membrane system are shown in Figure 4.This system is being tested in the laboratory. A major problem is damage of membranes during installation. Micro-operation procedures are being pursued to solve this problem.

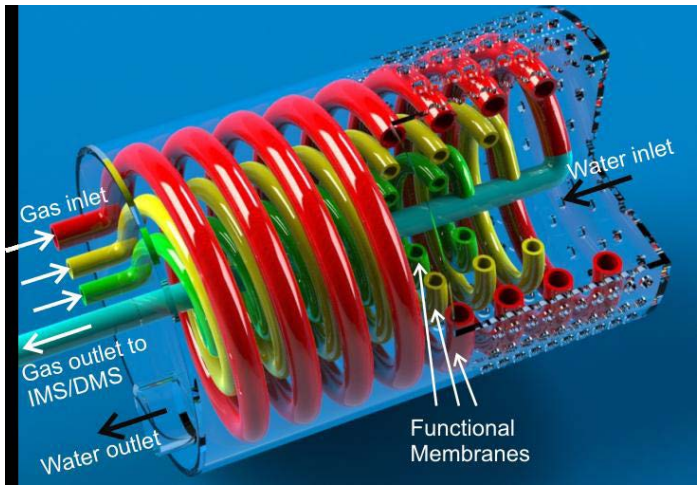

Figure 3. Illustration of membrane sampling system capable of multi-functional extraction of CHC from water.

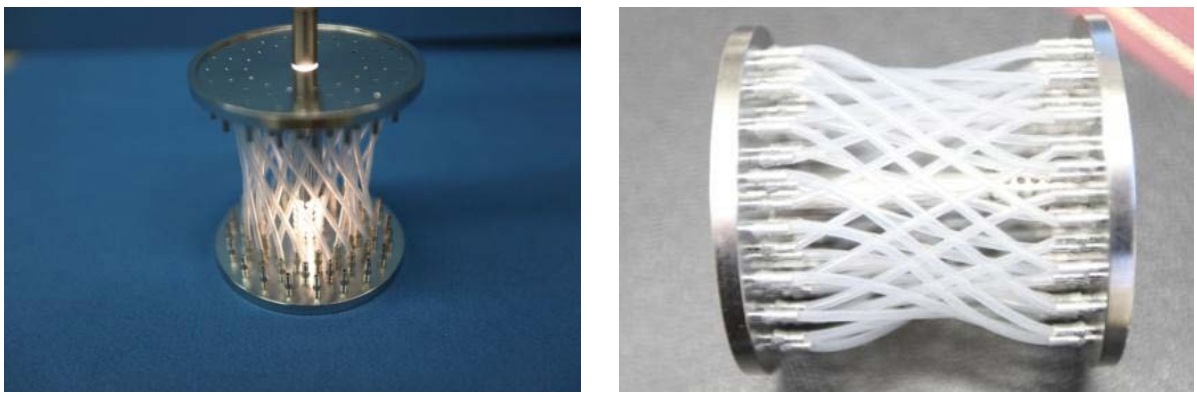

Figure 4. Images of multi-loop membrane extraction device.
First layer of membrane (left), and completed layers of membranes (right).

3.2 ION MOBILITY SPECTROMETRY

With the high probability of formation of both positive and negative ions from CHC, we fabricated a miniature linear IMS. Linear IMS refers to a technique based on the linear relationship between ion drift velocity (V_d) and an applied electric field (E) (Eiceman and Karpas, 2005). Generally the ions drift in a gas cell at ambient pressure and so can be used without the need to create a vacuum. Ions in a reaction region are extracted and injected as ion swarms into a drift region where separations occur through differences in V_ds of the ion swarms in an E of a few hundred volts per centimeter (V/cm). The drift velocities can be associated to molecular structure through the mobility coefficient (K) and linearly depend on the E:

$$V_d = KE \tag{1}$$

This separation by ion mobility creates selectivity for determination of chemical identity. In IMS, ions are characterized by collision cross section of ions with drift molecules, in contrast to a mass spectrometer where ions are characterized by mass-to-charge (m/Z) (Eiceman and

Karpas, 2005). The attraction of IMS includes operation at ambient pressure (no vacuum system), which yields efficient ionization and low power consumption.

Mechanical structure, electronics, thermal, and gas flows have been considered for the IMS-DMS analyzer, as shown in Figure 5. A feasible interface structure was designed so that ion paths driven by the E in IMS match to those given by the gas flow in DMS. Based on our simulation described above, major parameters for operating the analyzer have been determined to be as follows:

- The distance between two Bradbury-Nielson (B-N) gates: 56 mm
- IMS drift-tube diameter: 8 mm
- DMS gap distance: 0.5 mm
- DMS length: 40 mm
- Radio frequency (RF) maximum voltage: 0.5 kilovolts (kV)-2.0 kV
- RF frequency: 0.5-1 megahertz (MHz)
- DMS Flow rate: 0.3-1 L/min
- Voltage compensation voltage (V_C) bias: -50~50 V
- CV speed: 0.5-5 V/min

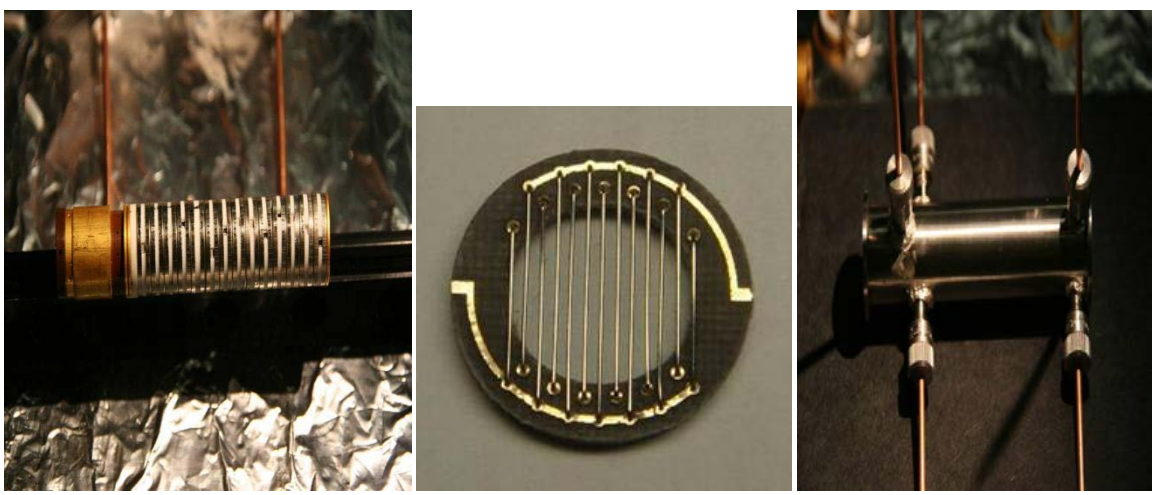

Figure 5. Inner elements of IMS-DMS analyzer (left), outer interface of IMS-DMS analyzers (right), and B-N gate (middle).

The parts of the IMS-DMS analyzer have been fabricated and assembled into a vapor separation system. The major elements of the separation system include (1) the atmosphere-pressure chemical ionization (APCI) chamber (Figure 6, left), (2) IMS drift channel electrodes (Figure 6, right) (3) two B-N gates (Figure 5, middle), (4) IMS-DMS interface (Figure 7), and (5) DMS filtration gap (Figure 8). More than 140 parts were made for this system. Some of these parts were obtained commercially by special requests and some were made in-house at ORNL.

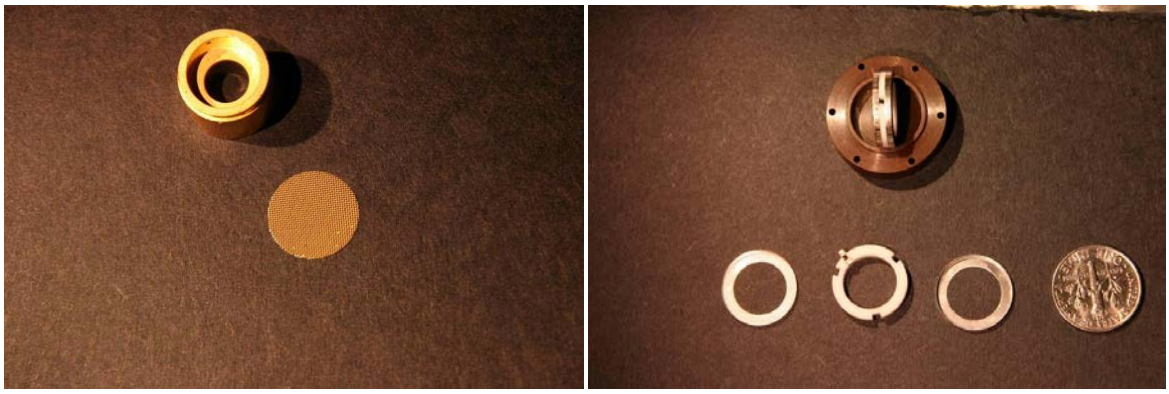

Figure 6. Photos of the atmosphere pressure ionization and reaction chamber (left).
(^{63}Ni isotope is coated in the inner surface as ionization source.)
One of 14 electrodes (right).
(Each electrode consists of an insulator ring, two conductor caps, and a miniature resistor.)

A few engineering aspects should be noted that were critical in making this system. A pair of B-N gates was adapted to control ions entering the DMS filtration gap and to select the IMS drift time. Electronics were made and tested for powering these gates. An important challenge encountered was how to relay the ion driver in IMS stage, which uses E, to the ion driver in DMS stage, which uses flowing gas. A unique IMS-DMS interface showed in Figure 7 was made so that the ion driver in IMS is overlapped with the ion driver in DMS by a flowing gas. This interface is expected to enable transfer of ions from the cylindrical IMS to the planar DMS without ion loss. Unique electrode contacts were also made for the assembly chamber (Figure 6, right) so that there is no leakage of air into the IMS-DMS separation channels while electrical contacts are firm and reliable.

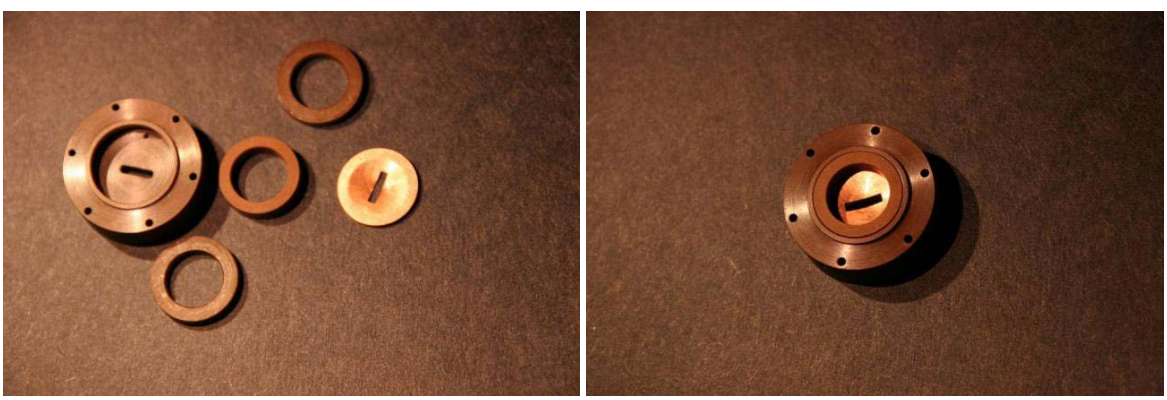

Figure 7. Parts (left) and assembly (right) of IMS-DMS interface.
(A ring of multi-gas channels was made to distribute the carrier gas evenly.)

The key factor for achieving the high resolution is to optimize B-N gate. A problem in the initial B-N gate occurred earlier. The gate failed when 300 V bias was applied between the inter-digitized grids. A new method was developed to fabricate the B-N gates. The method involved fabrication of inter-digitized grids on the same piece of a printed circuit board (PCB) (black polytetrafluoroethylene [PTFE]). The PCB can operate up to 120 ºC without emitting appreciable contaminants. The two silver rings are coated on the board as the bases for both positive and negative biases. The small 0.2 mm diameter holes were made in the silver rings and stainless

steel wires were soldered in the ring through the holes. All the wires are in the same plane, as shown in Figure 5, Middle. Six B-N gates were made using this method. They were tested and found to be functional and should be more suitable for use in harsh conditions.

A specialized IMS analyzer was made which consisted of an APCI chamber, a B-N gate, a drift tube, a Faraday detection plate, and a pre-amplifier. The analyte was first sent into the APCI chamber using the transport flow. The ionization source used was 5 mCi, ^{63}Ni. These ions were then injected by the B-N gate into the IMS drift channel. The home-made B-N gate consisted of 13 inter-digitized grids located in the same plane and supported by a circular PCB material with an OD of 14.8 mm. The IMS electrodes were made of stainless steel rings separated by alumina rings. The distance between the adjacent electrodes was 3.8 mm and the ID of the rings was 10.8 mm. Resistors of 1 Megaohm (MΩ) each with 1% variation were placed between adjacent ring electrodes. Electric potentials were distributed to these electrodes for generating a uniform drift field, as well as to the source electrode for sending ions close to the B-N gate. The drift gas had a flow rate of around 300 standard cubic centimeters per minute (SCCM) and was opposite to the ion traveling direction. The entire drift channel was temperature-controlled with a tape-heater. A home-made current-sensitive preamplifier was made with 10 kilohertz (kHz) bandwidth and had a gain of 2H109 volts per ampere (V/A). The output voltage was sent to a digital oscilloscope (Tektronix TDS2024B, 200 MHz) and a subsequent computer for recording.

3.3 GC/DMS ANALYZER

In a DMS analyzer, ions are carried with a flow of gas through a narrow gap between two electrodes. A high frequency, high voltage asymmetric waveform is applied between the electrodes resulting in an E that causes ions to undergo fast oscillations perpendicular to the gas flow. The ions consequently experience a slow net displacement toward the electrode based upon differences in Ks during the oscillations. Only the ions with a total transverse displacement less than the width of the distance between the plates will pass through the analyzer. Thus, an ion that can reach the detector through the drift gap correlates to a characteristic *compensation voltage*. A sweep of compensation voltages will provide a measure of all the ions in the analyzer and results in separation. Separation ability in DMS depends on differences in ion mobility at low and high Es (Shvartsbury, 2008). Ion V_d is understood to vary non-linearly for high E (E/N=100 Townsends, where E is the E and N is the density of neutral drift molecules):

$$V_d = K_0\big(1 + \alpha(E/N)\big)E \tag{2}$$

where $\alpha(E/N) = \alpha_1(E/N)^2 + \alpha_2(E/N)^4 + \alpha_3(E/N)^6 + \ldots$. In order to separate CHC that cannot be separated by linear IMS, ∀ needs to be different in the high field region.

In this project, with approval from Strategic Environmental Research and Development Program (SERDP) Environmental Restoration Program Manager, we obtained a GC/DMS analyzer from Sionex Corp (Anderson et al., 2008). The DMS filtration gap is shown in Figure 8. The GC/DMS, together with other elements, were integrated according the configuration shown in Figure 1.

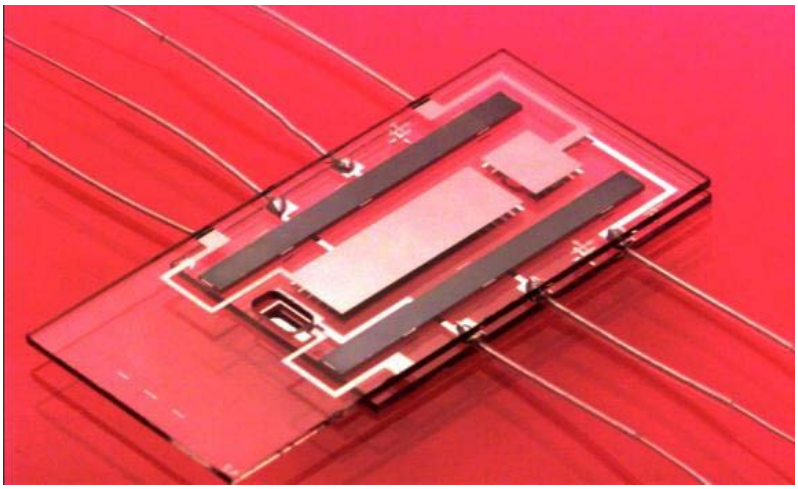

Figure 8. Sionex DMS filtration chip (Mosley, 2010).

4.0 MATERIALS AND METHODS

4.1 IDENTIFICATION BY ME-IMS

Figure 9 shows a typical negative-mode IMS spectrum of dry air at 50 °C where the major peak is $O_2^-(H_2O)_n$ and the satellite peak is $NO_2^-(H_2O)_n$. This IMS spectrometer is capable of achieving a resolution of R=33 in negative mode and R=41 in positive mode at 50 °C. R is defined as the peak drift time divided by the full width of the half maximum of the peak.

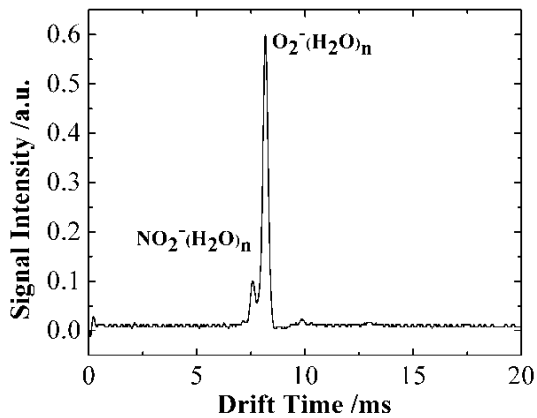

Figure 9. IMS spectrum for dry air flowing into a 50-cm PDMS membrane tube.
(Drift bias is -2000 V, Drift tube temperature is 50 EC [Du et al., 2010])

The clean membrane was immersed in a flask that contained 200 mL water and a selected contaminant, either TCE, PCE, or CH_3I with concentrations of 10 ppm (14.6 micrograms per liter [µg/L]), 10 ppm (16 µg/L), and 10 ppm (22.8 µg/L), respectively. Figure 10 shows the IMS spectra in negative mode for the three different contaminants. All reactant ion peak (RIP) positions are at 8.14 ms, produced by the drift field of (1800 V across 6.4 cm), indicating a reduced mobility of $2.36\times10^{-4}m^2\times V^{-1}\times s^{-1}$ of $O_2^-(H_2O)_n$. Interestingly the drift times for both TCE and PCE are the same, 7.14 ms, while the drift time for CH_3I is at 7.44 ms, characteristically different. We attribute the resulting negative ions to be those associated with halogen atoms, namely $Cl^-(H_2O)_n$ or $I^-(H_2O)_n$, with no effect of the carbon hydrogen constituents. It is known that the electron affinities for halogen atoms are high, leading to formation of negative halogen ions. Then the halogen ions interact with $H_2O(g)$ to form halogen-water complexes. The difference of the drift times between $Cl^-(H_2O)_n$ or $I^-(H_2O)_n$ is consistent with the difference of Cl and I masses.

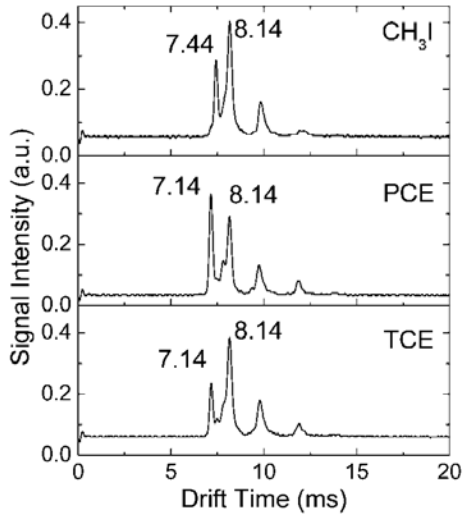

Figure 10. Negative mode IMS spectra for TCE, PCE, and CH_3I, spiked in water with concentrations of 10 ppm respectively (Du et al., 2010).

4.2 IDENTIFICATION BY ME-GC/DMS

In ME-GC/DMS experiments, a VF-624 capillary column, 5 meters long, was connected in-line between the preconcentrator and the DMS detector. The DMS includes a 5 mCi ^{63}Ni ionization source, two electric plates which were biased to the RF voltage and to a compensation voltage, and two electrode plates for collecting both positive and negative ions, respectively. GC/DMS operation procedures can be found in (Sionex Corporation, 2006) Reference 9. The final data recorded were in 2D domain, with DMS compensation voltage and GC retention time, (V_C, t_R), as identification parameters. For example, a 2D signal centered at retention time 80 s and compensation voltage -5 V will be expressed as (V_C, t_R) = (-5 V, 80 s). Data were analyzed based on a volumetric integration concept, that is, to sum up all the signal point values encompassed in a signal region formed by the retention time period and the compensation voltage span. Then the corresponding background reading was subtracted from the sum.

The experimental conditions, listed in Table 1, were used for this measurement. Except where noted, these conditions were used for all the experiments. Figure 11 shows 2D spectra for both positive (a) and negative (b) ions detected from 435 microgram per liter (µg/L) TCE (300 ppbv) and 490 µg/L PCE, respectively, spiked in water. As shown in the figure, TCE and PCE are identified by the 2D parameters, (V_C, t_R), for both positive and negative ions, where V_C is the compensation voltage and t_R is retention time. These ID parameters are listed in Table 2. The detected negative ions for both TCE and PCE are $Cl^-(H_2O)_n$ (n =1-3) monomers (Sionex Corporation, 2005), while the identity of the positive ions are not known at this point. Both polarities of the ions were detected at the same time. In fact, identification can be done by using either negative or positive ions alone. Not all molecules have simultaneous positive- and negative-ion formation under current conditions, as will be seen later. Therefore, the presence of both positive and negative ions for TCE and PCE allows independent confirmation of the identification.

Table 1. System parameters used in our experiments.

Carrier gas flow rate	150 SCCM
Trapping time	20 s
GC pressure difference	0.3 atm
Trapping pump flow rate	84.0 SCCM
Solution temperature	25EC
DMS detector temperature	120EC
DMS detector pressure	1 atm
DMS RF voltage	1100 V
DMS RF frequency	1.25 MHz
V_C span	-27 V~ +3V
V_C Step	0.3 V
Period per scan	1 s

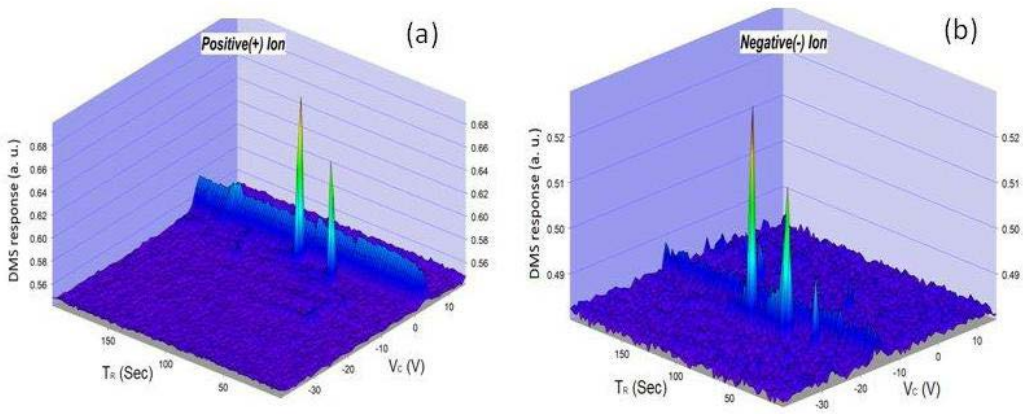

Figure 11. 2D GC/DMS spectra of 435µg/L TCE (300 ppbv) and 490µg/L PCE in water both in positive mode (left) and negative mode (right).

The signal intensity was found to be a function of permeation time, determined by the time needed for the contaminant to permeate through the membrane and to be carried into the analyzer. In our experiments, we used 3.5-minute permeation time, defined as the time after a fresh membrane is placed in water. In this permeation time, nearly 66% of the maximum intensity was reached. Unless described otherwise, the preconcentrator started to collect sample 3.5 minutes after the membrane was placed in sample liquid. Note that the selection of 3.5 minutes permeation time is the result of balancing sensitivity, trapping time, and analysis duty cycle.

trans-1, 2-DCE contaminants of 200-ppbv were spiked in water and were measured with both ME-GC/DMS and ME/IMS detectors. In ME-GC/DMS measurements, the DCE was identified with 2D parameters of (V_C, t_R) = (-21.11 V, 42.5 s) for negative and (V_C, t_R) = (-7.78 V, 42.5 s) for positive ions. Figure 12 (right) shows DCE spectra with respect to DMS compensation voltage for both positive- and negative-ion modes. Figure 12 (left) shows IMS spectra for both positive- and negative-ion modes. Unlike TCE and PCE, the peak intensity in positive-ion mode measured in DMS is much stronger than that in negative-ion mode. The larger amounts of ions

formed for *trans*-1,2-DCE was confirmed using IMS measurements, as shown in Figure 12 (left). Although the underlying reason for such preference is not known under current conditions, the use of positive ions can be considered more appropriate for the detection of *trans*-1,2-DCE.

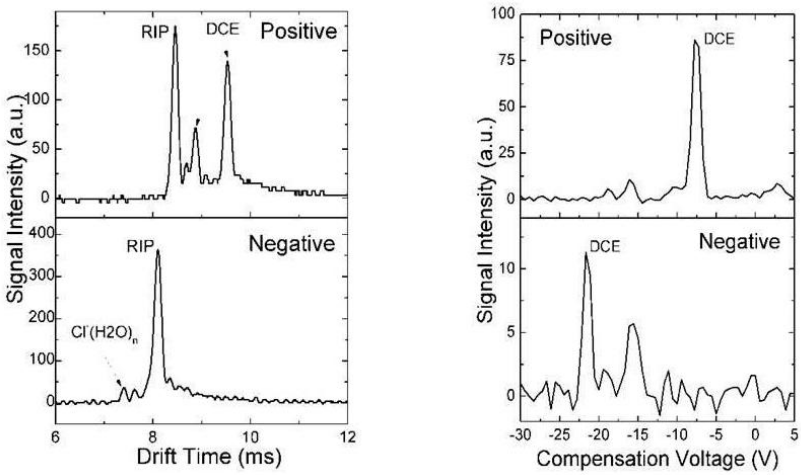

Figure 12. Detection of *trans*-1,2-DCE with IMS (left) (saturated headspace vapor) and membrane GC/ DMS system (right) (200 ppbv).

4.3 INTERFERENCE TEST

To reliably identify CHC, with the initial focus on PCE, TCE, and *trans*-1,2-DCE, the identification parameters should not be impacted by the presence of other molecules in water. We have tested co-interference, meaning detection of TCE with presence of other CHC, and foreign interference, meaning detection of TCE with presence of contaminants other than CHC. Figure 13 shows 2D spectra in both positive- and negative-ion modes for a mixture of solution consisting of PCE, toluene, TCE, benzene, CH_2Br_2, CCl_4, $CHCl_3$, and *trans*-1,2-DCE with 30 ppbv concentration each in water except for *trans*-1,2-DCE (60 ppbv).

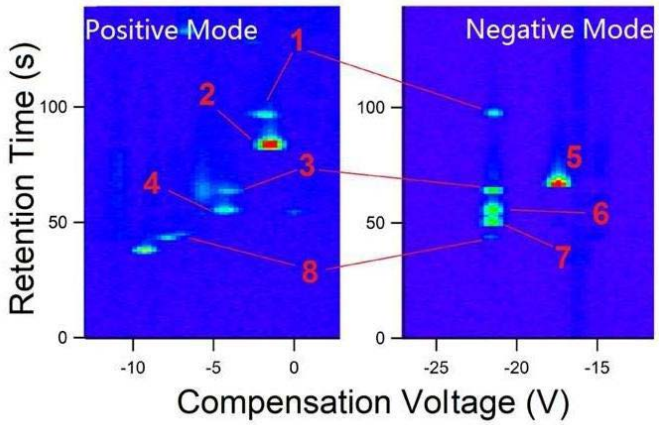

Figure 13. Separation of eight VOC mixed in water: PCE, Toluene, TCE, Benzene, CH_2Br_2, CCl_4, $CHCl_3$, and *trans*-1,2-DCE.

(All chemicals were simultaneously spiked in de-ionized water

with a concentration of 30 ppbv except *trans*-1,2-DCE 60 ppbv.)

Their identification parameters are listed in Table 2. It is shown that the identification parameter for TCE and PCE are the same as observed when they were alone in the water, as shown in Figure 11. Chloroform, carbon tetrachloride, benzene, and toluene were also separated and detected using this detector. All chlorine-related molecules that appeared in negative-ion mode gave rise to specific peaks at the same compensation voltage (-21.1 V), but at different retention times. This is due to the well-known formation of the same negative ions, $Cl^-(H_2O)_n$. The identities of these chemicals in water were verified with GC-mass spectrometry (MS) by a commercial firm, Analytical Chemistry Organization, Oak Ridge. Based on our re-producible data, we conclude that the identification parameters were not changed by the co-existence of different type of molecules under the conditions described in Table 1. These results suggest that there are no competitive reactions in the water, PDMS membrane, or vapor flow through the remainder of the system. However, one caveat is that the compensation voltage can be shifted from -21.1 V to -21.7 V for an aging carrier-gas drier, probably relating to a higher moisture level.

Table 2. Identification parameters for different chemicals with GC/DMS.

Chemical Name	Negative Mode (V_C [V], Retention Time [s])	Positive Mode (V_C [V], Retention Time [s])
TCE	(-21.1, 62.8)	(-3.3, 62.8)
PCE	(-21.1, 97.2)	(-1.1, 97.2)
trans-1,2-DCE	(-21.1, 42.5)	(-7.8, 42.5)
Benzene	Not detected	(-4.4, 56.6)
Toluene	Not detected	(-1.1, 83.0)
CCl_4	(-21.1, 54.9)	Very small
$CHCl_3$	(-21.1, 48.6)	Very small

It is noted that some VOCs, such as benzene and toluene, gave rise to only positive ions, while CCl_4 and $CHCl_3$ gave rise to mostly negative ions. Interestingly, the molecules focused on for this work (TCE, PCE, and DCE) gave rise to both positive and negative ions. The useful implication is that, we can use negative-ion mode to identify and quantify CHC and positive-ion mode to confirm the identification.

Figure 14 shows GC-IMS 2D spectra for both positive-ion and negative-ion modes for 28 chemicals spiked in water at 100 ppb levels. It is clear that the ME-IMS technology is capable of identifying these chemicals without interference. Based on laboratory tests, the LOD for TCE is 0.37 ppbv (0.54 µg/L) for a 20-second (s) sampling time. Under the same experimental conditions, the LOD for PCE with a sampling time of 20 s is 1 ppbv (1.62 µg/L).

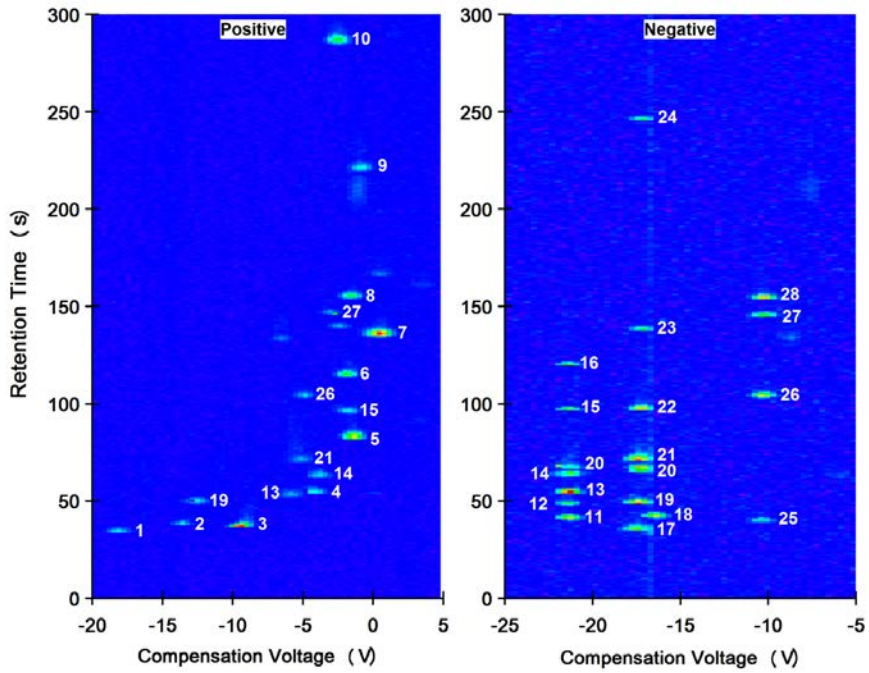

Figure 14. 2D plots from the ME GC DMS analysis of the mixture of 28 chemicals in water. (The contours show ion current as a function of retention time (vertical axis) and compensation voltage (horizontal axis) for (a) positive and (b) negative ions. Peak # corresponds to (1) methanol, (2) acetonitrile, (3) acetone, (4) benzene, (5) toluene, (6) o-Xylene, (7) chlorobenzene, (8) bromobenzene, (9) 1,2-dichlorobenzene, (10) nitrobenzene, (11) dichloromethane, (12) chloroform, (13) tetrachloromethane, (14) trichloroethylene, (15) perchloroethylene, (16) chlorohexane, (17) ethyl bromide, (18) carbon disulfide, (19) bromopropane, (20) dichlorobromomethane, (21) bromobutan, (22) dibromochloromethane (23) bromoform, (24) carbon tetrabromide, (25) iodomethane, (26) iodobutane, (27) iodopentane, and (28) di-iodomethane.)

4.4 SENSITIVITY TEST

The sensitivity of the ME GC/DMS detector is related to many factors, including membrane dimensions, type of analyte, permeation temperature and pressure, carrier gas flow rate in the membrane, type of adsorbent in the preconcentrator, adsorbent temperature, sampling time, sampling flow rate, and many other minor factors. Optimized conditions for membrane permeation have been reported in our previous work (Sionex Corporation, 2005). In this work, we optimize the sensitivity by varying sampling conditions in the preconcentrator. It was found that the sampling flow rate of ~84-SCCM that drives sample through the adsorbent gave rise to the best detection sensitivity.

Signal intensity of the GC/DMS detector in response to various sampling times for 5-ppbv TCE-water solutions was measured and converted into the LOD, as shown in Figure 15. Identification parameters, (V_C, t_R)=(-21.1 V, 62.8 s), were chosen so that the signal only represents TCE detected in the negative-ion mode. The intensity was determined by the integration of the TCE peak over both DMS compensation voltages and GC retention times. LODs were obtained by calculating signal-to-noise ratio (S/N) on a basis of N equal to 3 times the standard deviation.

As expected, the LOD decreases as the sampling time increases. The trapping-time dependence of sensitivity suggests that the preconcentrator is a primary factor responsible for higher sensitivity over that given with ME-IMS. The LOD for TCE is 0.37 ppbv (0.54 µg/L) for a 20-s sampling time. Under the same experimental conditions, the LOD for PCE with a sampling time of 20 s is 1 ppbv (1.62 µg/L). According to the U.S. Environmental Protection Agency (USEPA) Method 8260B, the LODs of a purge and trap GC/MS for TCE and PCE are 0.19 µg/L and 0.16 µg/L, respectively. In this in-situ detector, we achieved about 0.32 µg/L for TCE at the 90-s sampling time, as shown in Figure 14, very close to the USEPA 8260B limits.

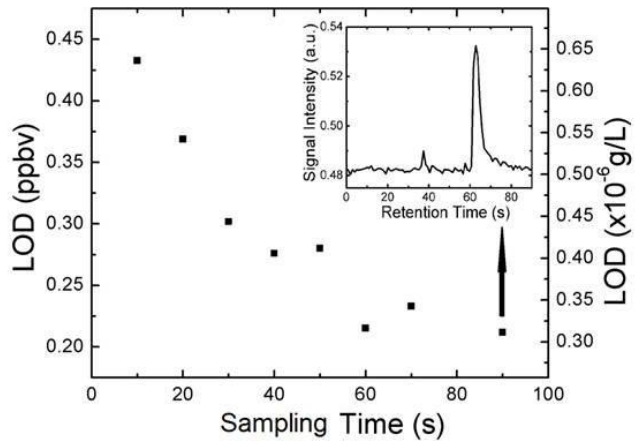

Figure 15. LODs for TCE as a function of sampling time (5 ppbv, negative ions).
(Inset: GC spectrum at DMS compensation voltage of -21.1 V with sampling time of 90 s.)

4.5 DYNAMIC RANGE AND CALIBRATION CURVES

Detector response to TCE concentration varying from 3 ppbv to 2 parts per million by volume (ppmv) in water has been studied. Figure 16 shows retention-time spectra in positive-ion mode (left) and negative-ion mode (right) for TCE spiked in water at various concentrations. The DMS compensation voltages were chosen to be -3.3 V and -21.1 V for positive- and negative-ion spectra, respectively. Therefore the peaks at 62.8 s represent TCE identification. At a lower concentration (70 ppbv), TCE only shows a single peak in both spectra. However, at a higher concentration, a tail at longer retention times appeared, and is especially pronounced in negative-ion mode. When TCE concentration increases to above 400 ppbv, the formation of $Cl_2^-(H_2O)_n$ dimmers compete with formation of the monomers. This competition leads to a sharp decrease in the $Cl_2^-(H_2O)_n$ monomer intensity at 62.8-s retention time. While the reasons responsible for the formation of both tailing feature need further investigation, it was confirmed that this feature is a direct response to TCE in water. Similar phenomena of “tailing” were observed for PCE, as shown in the supporting information, but at much higher concentrations than for TCE. This phenomenon poses difficulties for the quantification of TCE and PCE in negative ion mode at high concentrations. Alternatively and fortunately, we can use positive-ion mode for quantification at higher concentrations.

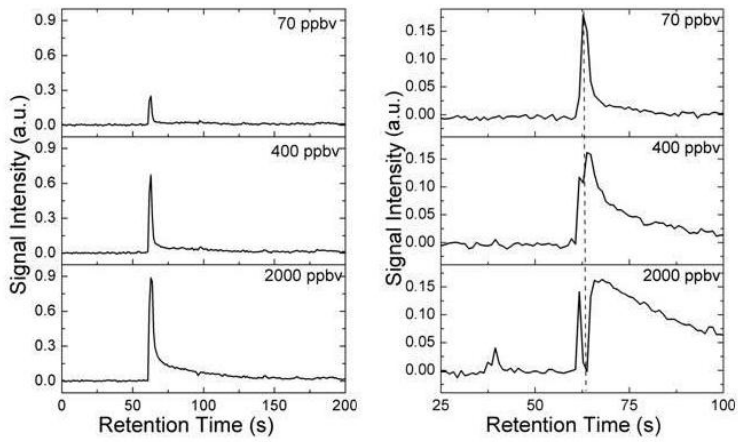

Figure 16. TCE tailing and cracking effects in negative mode (right) and corresponding positive mode signals (left).

Figure 17 (left) shows integrated intensity of positive-ion TCE peak as a function of concentration varying from 30 ppbv to 2 ppmv. Figure 7 (right) shows integrated intensity of TCE peak in negative-ion mode as a function of concentration varying from 3 ppbv to 300 ppbv. The curves are the fits to two exponential functions and are not linear. At low concentrations (<100 ppbv), the TCE detection sensitivity was higher in negative-ion mode than in positive-ion mode. When the concentration increases to above 100 ppbv, the negative-ion intensity becomes saturated. This is probably due to the "tailing" and the dimer formation. However, at higher concentrations, the positive ion intensity continues to increase as a function of TCE concentration, although not linearly. Therefore we can achieve a large dynamic range by combining both positive- and negative-ion measurements. When the concentration is below 100 ppbv, we can use negative-ion mode for quantification. When the concentration is above 100 ppbv, the positive-ion mode can be used for quantification. In addition, both modes can be used to confirm the identification of the analyte. Similar measurements were carried out for PCE as shown in the supporting information. The same analogy for TCE quantification can be applied to PCE quantification over a large dynamic range.

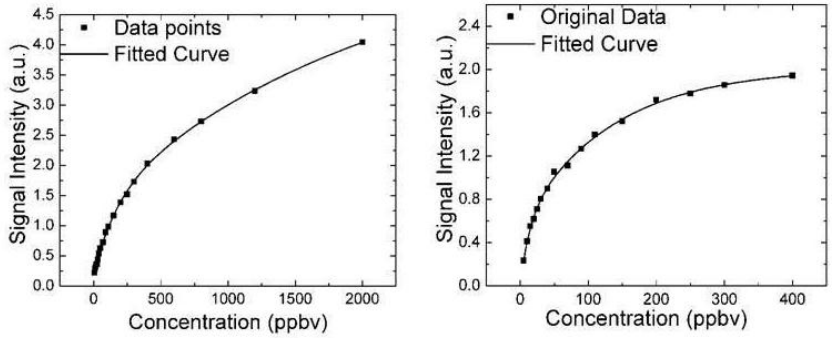

Figure 17. TCE signal intensity as a function of concentration.
Positive ion mode (left). Negative ion mode (right).

Such nonlinearity was obtained from the two different analyzers with the same membrane sampling method. Then it is reasonable to suggest that the non-linearity is not due to detector, instead, due to the analyte's nonlinear permeation through the membrane. To confirm this, experiments were conducted at ten different dilutions by varying the dilution flow (DF) rate. Volumetrically integrated signal intensity was plotted against DF and shows the linear relation between signal intensity and DF. Such linearity reflects that the analyzer's response is linear and that non-linearity is due to concentration dependent permeation. It is understandable that at a high concentration, molecule-molecule interactions may reduce permeability. Because of this nonlinearity, quantitative calibration has to be done by measuring the entire concentration curve. Normal proportionality comparison cannot be used for calibration under this operational scenario.

5.0 RESULTS AND DISCUSSION

On September 19, 2011, the team carried out field tests at NASA SSC. The purpose was to demonstrate a home-developed prototype in-situ, compact, stand-alone monitor for monitoring CHC in groundwater in real groundwater wells. We also wanted to identify problems that need to be solved for reliable identification and quantification of contaminants in real environments. Figure 18 shows the field team.

Figure 18. Photos of field testing in NASA SSC.
(Inset 1: Portable ME GC-DMS monitor;
Inset 2: Sending ME assembly to the groundwater well;
Inset 3: Bees and their nest located on the cover of the well.)
(Researchers: A, Shasha Cheng; B, Xixi Liang; C, Wendy Robinson;
D, NASA supporting staff; E, John Hughes; and F: Jun Xu.)

The monitor consists of a ME assembly, which contacts water directly, a preconcentrator, and a portable GC/DMS. In 06-11 MW groundwater well, the main characteristics are (a) TCE concentration is low (386 μg/L, reported in May 2011); (b) groundwater recharge is 0.03 feet/minute, very slow; and (c) the average water temperature is 21.0 EC. For this well, the monitor was first tested as a function of water depth. The membrane extraction assembly was placed at different water depths of 6, 7, 8, 9, and 10 meters from the top of the well. Then the monitor was fixed at 10-meter depth and tested as a function of time when the pump was extracting water out of the well. The testing was conducted every five minutes.

In 06-12 MW, (a) TCE concentration is high (2600 μg/L in May 2011); (b) recharge rate is almost instantaneous; and (c) the average temperature is also 21.0 EC. No depth profile test was

done because 06-12 MW is deeper than 06-11 MW. In this case, the monitor was fixed at 10-meter depth. First, water sample was tested at three different times of 3, 8, and 13 minutes after the well cover was exposed to air. Then, water was monitored as a function of time when the pump was extracting water out of well and groundwater was recharging simultaneously. The tested was conducted also every 5 minutes.

Weather conditions consisted of rain in the morning, sunny at mid-day and stormy conditions in the afternoon, during the time of the testing. Before the tests both wells were covered and locked for a period of a few months. During this time a wasp's nest was built in the outer cover of the well, as shown in Insert 3 of Figure 18.

5.1 CONTAMINANT IDENTIFICATION

5.1.1 06-11 MW

Identification was conducted using 2D separation. The first dimension is the compensation voltage, V_C, and the second dimension is gas-chromatographic retention time, t_R. Figure 19 shows the 2D plots of negative-ion mode for 10m-depth groundwater sensed in 06-11 MW. TCE was identified at (V_C, t_R) = (-21.1 V, 90.1 s) for negative ions and = (-2.8 V, 90.1 s) for positive ions. TCE is the dominant contaminant in this well. The other large peak is associated with a membrane solvent.

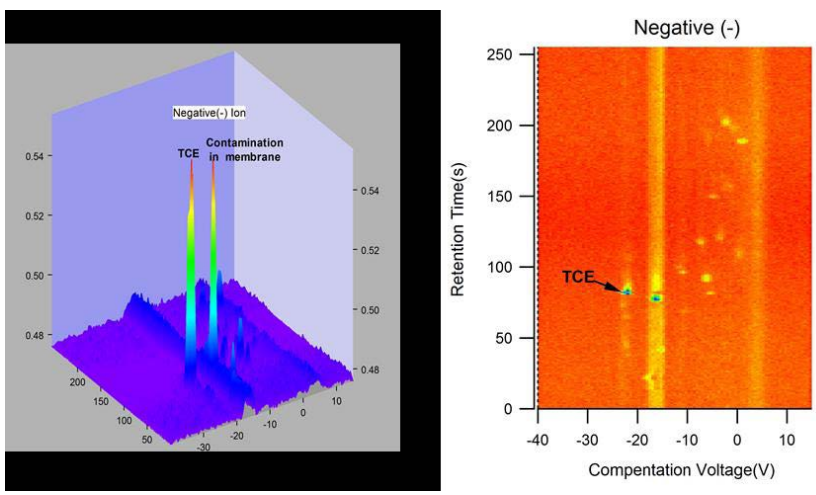

Figure 19. 2D Spectra depicting TCE contamination detected by membrane GC/DMS in specific ion mode

Monitor was set at 10-meter depth of 06-11 MW well.

5.1.2 06-12 MW

Figure 20 shows 2D plots of both negative- and positive-ion modes for 10-meter depth groundwater in 06-12 MW. TCE was identified at (V_C, t_R) = (-22.2 V, 87.0 s) for negative ions and = (-2.8 V, 87.0 s) for positive ions. It is noted that another major contaminant at (-21.1 V, 46.6 s) was also observed in this well. This peak was identified in lab to be CH_3Cl (methyl

chloride/Freon 40) ions. Figure 21 is the planner view of the 2D spectra of the same data as Figure 20.

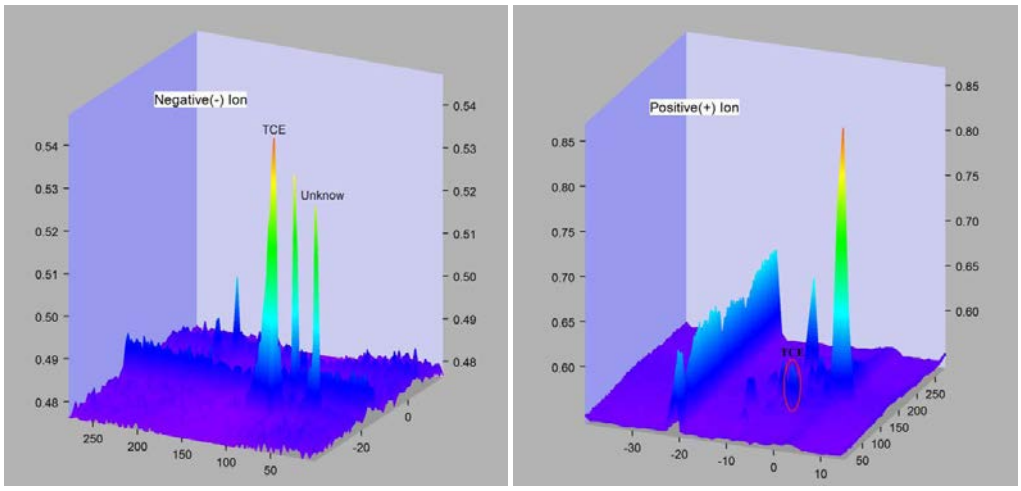

Figure 20. 2D spectra of contaminants in 06-12 MW for negative (left) and positive mode (right).
(The monitor was placed at 10 m depth from the well top.)

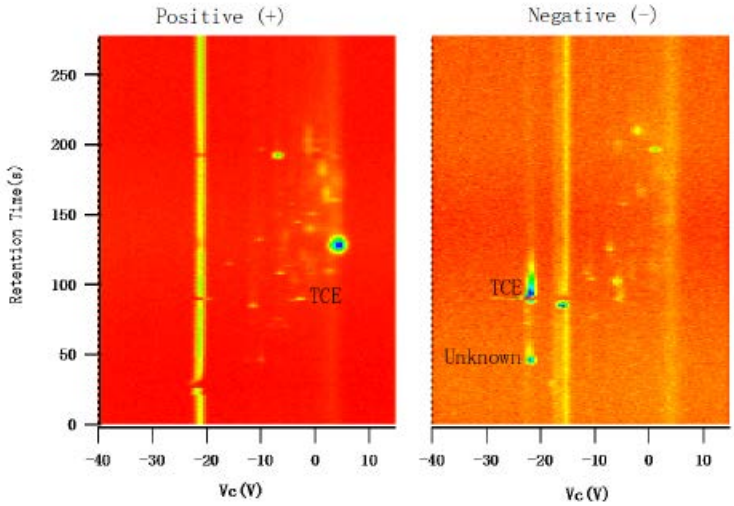

Figure 21. Planar view of 2D spectra.
(These are the same data as Figure 20.)

5.2 CONTAMINANT QUANTIFICATION

Quantitative analysis was conducted by the following steps: First in laboratory, the curves between monitor response and TCE concentration were measured for both positive- and negative-ion modes.

Table 3. TCE concentrations and ID parameters for MW 06-11 and MW 06-12 wells.

Well Test#		Retention Time(s)	Compensation Voltage(v)		Concentration (ppb)
			Positive	Negative	
MW 06-11	Test 1	85.079	-2.78	-22.78	413 (602 µg/L)
	Test 2	90.1.11	-2.78	-21.1	354 (516 µg/L)
MW 06-12	Test 1	93.136	-2.78	-22.22	2435 (3550 µg/L)
	Test 2	87.009	-2.78	-22.22	2684 (3918 µg/L)

For MW 06-11well, two tests were conducted under the same conditions. In either negative or positive mode, there is just one peak corresponding to TCE. TCE peak areas in positive mode of two tests are 0.12185 and 0.11068. According to the calibration curve, the concentrations of TCE should be 413 ppb and 354 ppb, respectively. On May 17, 2011, this well was tested by the NASA team to have 386.00 µg/L of TCE. Our test result is close to what expected for this well.

For MW 06-12, two tests are almost identical. TCE peak areas of two tests in positive mode are 0.46098 and 0.49181, which are not in the range of the calibration curve for TCE. With extrapolation of the calibration curve, we calculated the concentrations of the TCE in the two tests to be 2435 ppb and 2684 ppb. On May 17, 2011, this well was tested by the NASA team to have 2600.00 µg/L of TCE. Again our test is close to the NASA standard test result.

A caveat is that our measured concentrations for both well are higher than SSC test TCE concentrations obtained from GC/MS. A speculation is that our method combines sampling and test steps without middle processing and shipping. During these middle processes, TCE may be evaporated due to unexpected conditions. Further comparison tests should be made to clarify this caveat.

5.3 DEPTH MONITORING

For MW 06-11 well, we measured various TCE peaks by placing the monitor at different depths of water. Figure 22 shows tested depths of 6, 7, 8, 9, and 10 m from the well top and their TCE concentrations. A general trend of TCE concentration is TCE (at 10 m)>TCE (at 9 m)>TCE (at 6 m)>TCE (at 7 m)>TCE (at 8 m). Then the monitor was fixed at the 10 m position, TCE was measured as a function of time when the “old” water was been pumping out. The pumping time-profile represents and confirms the depth profile because this well has almost no re-charging somehow. Both measurements show three TCE concentration zones: the near surface zone (at 6 m), near active groundwater zone (at 10 m and 9 m), and the zone in the middle (at 7 m, and 8 m). It has been found that both water zones near surface and close to the “true” groundwater have much higher TCE concentrations than that measured in the middle zone. The higher concentration in the near surface zone makes sense because TCE has higher vapor pressure than water. TCE evaporates to the well head space and balanced with the surface water when the well is covered. As a result, the water near surface exhibits the high TCE concentration. It also makes sense for the highest TCE concentration in the water that is close to the true groundwater because this is where the contaminant plume originates.

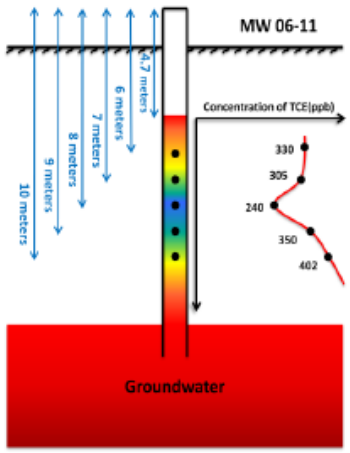

Figure 22. Distribution of TCE concentration as a function of depth for MW 06-11 well measured by the membrane GC/DMS monitor.

Besides positive results as described above, many problems were discovered. These problems are associated either with our monitor, practical unpredicted environments, or inexperience in field test. Here lists the main problems.

1. One of identification parameters, retention time, varied in field in a large uncertainty: 11%, much worse than that in lab. In a lesser problem, the V_C varied within less than 5%. These uncertainties may originate from the short duty cycle, as stated above, and from the moisture/temperature uncertainties in field.
2. Some quantification is not accurate in this test because the instrument temperature was not stabilized due to the short duty cycle and the high atmospheric temperature. Correct duty cycle should be between 20 and 30 minutes. This will be taken care in future tests.
3. This instrument was designed for low-concentrations of CHC in water. For high-concentration wells (<2 ppm), the instrument response tends to be saturated. For practical monitors capable of dealing a large dynamic range, an in-field dilution mechanism should be considered in the future.

6.0 CONCLUSIONS AND IMPLICATIONS FOR FUTURE RESEARCH

6.1 CONCLUSIONS

- ***Identification is reliable.*** No interference from presence of other containments was observed. This reliability is given by the 2D separation of the technology. A small variation of ID parameters was observed in the field environments and can be corrected by automatic adjustments to the RIP, which is also affected by the environments in the same manner as TCE.

  Suggestion: Simultaneous measurements of ID parameters for both reactant ions and sample ions should be made. The relative differences will be used to identify contaminants. This capability will be built-in into the monitor software. When this adjustment is addressed, there is no need to put more effort to improve resolution.

- ***Quantification is excellent in laboratory, but not highly accurate in field under current conditions.*** From laboratory experiments, the LOD can be as low as 0.37 ppbv for TCE. Similar order for other chlorinated solvents. The monitor is very reliable for quantification at least in laboratory. However, quantification was affected by both groundwater temperature and pressure in field testing experiments. The main problem is that the membrane permeation used in conversion of aqueous TCE to vapor TCE behaves differently at various temperature and pressure, as expected.

  Suggestion: The monitor should be modified to enable analysis of samples under a variety of environmental conditions, including large variations in temperature and pressure. Water temperature and pressure will directly affect contaminant permeation through the membrane, complicating analysis. Therefore, quantification curves for various temperature and pressure should be obtained and used for calibrating field concentration with corresponding temperatures and pressures.

- ***ME-GC/DMS monitor may need to work with non-linear quantification curves.*** Bad news is that it has been found that the relation between instrument response and contaminant concentration is non-linear. At a higher concentration, the response seems slower. This has been verified in many lab tests. The science behind this behavior is believed to arise from non-linear permeation rate of CHC in the membrane. Good news is that these non-linear curves are stable and reproducible. Non-linear curves can be used as calibration.

  Suggestion: The quantification curves should be measured for given conditions, such as temperature, and stored in the monitor computer. In a field test, one of the curves with the same/approximate conditions in laboratory should be called to correlate the monitor response to the concentration in the curve. Lab works, software modification, and field test will be conducted to validate this concept.

- ***Dynamic range is limited.*** Current dynamic range for TCE detection is from 0.5 ppbv to 2000 ppbv. Within this range, 0.5-200 ppbv is covered by the negative-ion mode, while 200-2000 ppbv is covered by the positive ion mode. In many groundwater wells, such as those in NASA SSC, the TCE concentration is higher than 2000 ppbv.

  Suggestion: Our plan to solve this problem is to have a dilution mechanism made so that our monitor can deal with high concentrations greater than 2 ppm. It is a misunderstanding that this ME-IMS monitor is only good for high concentrations, not adequate for lower concentrations. Fact is exactly opposite: the monitor is more reliable to low concentrations (0.5-200 ppbv). In this NASA SSC field test, TCE concentration was much greater than 200 ppbv. Therefore we did not use the negative-ion mode. As shown in Figure 17 (right), negative-ion mode is reliably used to quantify low concentrations.

- ***Monitor Dimensions are too large for some practical groundwater wells.*** Our current ME-IMS monitor was designed for 4-inch diameter of groundwater wells. As informed in NASA SCC, many wells are 2 inches in diameter.

  Suggestion: Monitor dimensions will be reduced and optimized to address the most common in situ sampling scenarios. In addition, the future 2-inch-diameter monitor should add capability of measuring water temperature and depth from the surface.

6.2 IMPLICATIONS FOR FUTURE RESEARCH

Additional issues and considerations toward the future demonstration validation of this technology include:

- Delineation of the range of concentrations for the various chlorinated hydrocarbons capable of confidently being determined by this field sensor in various, typical field sampling conditions. Such confidence would be based on validation testing in accordance with DoD sampling and analysis methodologies and associated quality assurance goals and objectives.

- A clear understanding of the long-term operational cost effectiveness of this field sensor. The cost analysis should include all direct and indirect costs, operational ruggedness and required maintenance, QA/QC issues and requirements, and capability of fulfilling ESTCP Cost and Performance Guidance requirements (http://www.serdp-estcp.org/Investigator-Resources/ESTCP-Resources/Technical-Reports).

- Identification of potential interferences that might be encountered both in a typical field environment as well as in those field conditions considered harsh. Such interferences could be anthropogenic (e.g., co-contaminants and their respective concentrations) or naturally occurring (e.g., total dissolved or

suspended solids, selected cations and anions, pH) with the impact of these interferences further defined through sensitivity analyses.

- Provision of clear and supportable analytical results capable of clearly differentiating among the chlorinated organic compounds typically encountered at DoD groundwater remediation sites; in particular, the ability to reliably identify and quantify analytical results for PCE, TCE, both *cis*- and *trans*-DCE, vinyl chloride and ethenes in variable groundwater conditions. Such analytical results also might entail the ability to more definitively identify Tentatively Identified Compounds (TICs) without the need for confirmation in a laboratory setting.

7.0 LITERATURE CITED

Almquist, C.B., and S.J. Hwangb. 1999. Journal of Membrane Science, 153, 57-69.

Anderson, A.G., K.A. Markoski, Q. Shi, S.L. Coy, E.V. Krylov, and E.G. Nazarov. 2008. Processings of SPIE, 6954, H9540-H9540.

Appelhans, A.D., and D.A. Dahl. 2002. Int J. Mass Spectrom, 216, 269-284.

Banat, F.A., and J. Simandl. 1996. Chemical Engineering Science, 51, 1257-1265.

Eiceman, G.A., and Z. Karpas. 2005. Ion Mobility Spectrometry, 2nd ed.; CRC Press: Boca Raton, FL.

Jun, X., and L. Yuan. 2009. Int. J. Ion Mobil. Spec. 12, 149-156.

Mosley, S. 2010. Forensic applications of differential mobility spectrometry.

Ohshima,T., Y. Kogami, T. Miyata, and T.J. Uragami. 2005. Journal of Membrane Science,, 260, 156–163.

Shvartsbury, A.A. 2008. Differential Mobility Spectrometry: nonlinear ion transport and fundamentals of FAIMS, 1st ed.; CRC Press: Boca Raton, FL.

Sionex Corporation. 2005. MicroAnalyzer™ Series Product Manual.

Y. Du, W. Zhang, W. Whitten, H. Li, D.B. Watson, and J. Xu. 2010. Analytical Chemistry, 82, 4089-4096.

Yeoma, C.K. S.H. Lee, H.Y. Song, and J.M. Lee. 2002. Journal of Membrane Science, 198, 129–143.

APPENDIX A

MODELING

A.1 Monte Carlo Simulation of IMS-DMS Analyzer

Monte Carlo calculation codes have been developed for simulating ion trajectories in DMS and IMS. In our proposal, the filtration gap for DMS was proposed to be cylindrical. However, based on insights provided by simulations, the filtration gap was changed to planar because a planar gap was found to have a higher resolution. An IMS-DMS analyzer was designed based upon this principle. A detailed description is given below.

In DMS simulations, a Monte Carlo method may be used to model ion–gas collisions. The collisions between the ions and gas atoms are assumed to follow the hard-sphere collision model (Appelhans and Dahl, 2002). The velocity of an ion in the center-of-mass frame before and after a collision is given as the difference of:

$$\vec{V} = \vec{V}_{lab} - \vec{V}_{cm} \tag{3}$$

$$\vec{V}' = \left(\left|\vec{V}\right| sin\ \theta\ cos\ \varphi, \left|\vec{V}\right| sin\ \theta\ sin\ \varphi, \left|\vec{V}\right| cos\ \theta\right) \tag{4}$$

V_{Lab} is the ion velocity in the laboratory frame and V_{cm} is the velocity of the center-of-mass. Due to the constraints of momentum and energy conservation, the magnitudes of ion velocities in the center of mass frame before and after a collision are the same. θ and φ are the azimuth and elevation angles, respectively. These angles after each collision are independent of one another and are determined using the random number generator:

$$cos\ \theta = 2Rand() - 1 \tag{5}$$

$$\varphi = 2\pi Rand() \tag{6}$$

where Rand () produces a random number between 0 and 1. After each collision, the new ion velocity was converted back into the lab frame. The ion velocity determined from a collision is used as the ion velocity for the next step. SIMION then recalculates the ion velocity after each ion step before the ion encounters another collision. The relative difference between ion velocity and the gas velocity in the laboratory frame was used for determining collision probability, as discussed below.

$$P = 1 - e^{-V_d \Delta t/\lambda} \tag{7}$$

$$\vec{V}_d = \vec{V}_{ion} - \vec{V}_{gas} \tag{8}$$

Utilizing the new simulation codes, we have studied IMS-DMS separation methods. Previously we proposed to use a cylindrical DMS filtration gap. However, our simulations indicate that a planar gap attached to the IMS exit increase the number of ions passing into the DMS gap. A

higher resolution (R = 32) was found for a 2-mm planar gap than that for a 2-mm cylindrical gap. Simulations show that there is ion focusing in cylindrical gap while such focusing is absent in the planar gap. This difference explains the higher resolution for the planar gap. Based on these results, we have made a change to the IMS-DMS structure from the proposed cylindrical one.

A.2 Separation Principles

In support of this work, the investigators made an important contribution to DMS analytical theory. This work has been published in Int. J of IMS (Jun and Yuan, 2009). Below we describe the details of the theoretical work.

In a DMS analyzer, an asymmetric periodic voltage, V(t), which should satisfy the following condition, is applied to the filtration gap:

$$\int_0^{\tau} V(t)dt = 0, \tag{9}$$

where τ is the period of the pulsed E. V(t) can be a time-dependent square waveform consisting of a high voltage (V_H) having a duration of τ_H (referred as high-field phase) and a low voltage (V_L) having a duration of τ_L with the opposite polarity to V_H (referred to low-field phase). For this square waveform, Eq. (9) can be expressed as:

$$V_H\tau_H + V_L\tau_L = 0 \tag{10}$$

The displacement (D) of an ion in the direction perpendicular to the gas flow direction over the time of one period of the asymmetric voltage is given by:

$$D = K_H \frac{V_H}{d}\tau_H + K_L \frac{V_L}{d}\tau_L\ , \tag{11}$$

where d is the gap height in the Y-direction, and KH and KL are the Ks of the high- and low-field phases, respectively. If $K_H = K_L$, there is no vertical displacement (D = 0) because (V_H, τ_H) and (V_L, τ_L) satisfy Eq. (10). In general, the low field mobility of the ion is independent of the field, while the mobility in a high field is dependent on the field and thus is different from the low-field value:

$$K_H = K_0\left[1 + \alpha\left(\frac{V_H}{d}\right)\right], \tag{12}$$

$$K_L = K_0. \tag{13}$$

Consequently, there is a net displacement of the ion towards one of the electrodes. In order to control such a displacement, a small voltage is superimposed on the asymmetric periodic voltage to compensate the displacement. For a given square waveform (V_H, τ_H) and (V_L, τ_L) and a constant V_H, the compensation voltage is:

$$V_c = V_L - V_{sL} \tag{14}$$

where V_L is the low-field voltage in the square waveform and V_{sL} satisfies the constraint given in Eq. (10).

In order for a desired ion to pass through the filtration gap, the compensation voltage that can cancel the vertical displacement of the ion is determined by:

$$\left(K_0 \frac{V_c}{d}\right)\tau + \left(K_H \frac{V_H}{d}\tau_H + K_L \frac{V_L}{d}\tau_L\right) = 0 \tag{15}$$

where $\tau = \tau_H + \tau_L$. Substituting equations (12), (13), and (10) into equation (15), we obtained an analytical expression for the characteristic compensation voltage for the case of square waveforms:

$$V_c = -\frac{\tau_H V_H}{\tau}\alpha(V_H) \tag{16}$$

Eq. (16) shows that V_C is directly proportional to the non-linear K $\forall$. Thus V_C can be used to determine the mobility difference under the high-field and low-field conditions. The values of $\forall$ for chemical species are generally small for a practical E. Eq. (16) indicates that the factor, $\tau_H V_H/\tau$ magnifies $\forall$ and allows chemical separation. Eq. (16) also shows that V_C is proportional to the relative duration (τ_H/τ) of the high-field phase.

A maximum RF voltage of 600 V, namely V_H, was applied to the upper electrode with the waveform shown Figure 23(a). The RF was 500 kHz in this simulation. The carrier gas had a flow rate of 0.8L/min. The ion moved on average downward during the high-voltage phase, and back up during the low-voltage phase. The random motion was observed for the both phases due to ion-gas collisions, as shown in the insert. The random motion was more pronounced in the low-voltage phase than in the high-voltage phase. This is because the axial velocity of the ion is slower in the low-voltage phase. So the diffusive random motion is relatively larger.

Figure 23 (b), (c), and (d) show ions trajectories with 0V, -3V, and -6V compensation voltages. It can be seen clearly that, at a correct compensation voltage, -3V, the most ions can pass through the filtration gap and be collected. The lower compensation voltage (-6V) drove the ions drifted towards the lower electrode; while the larger compensation voltage (0V) drove the ions towards the upper electrode. These ions would be neutralized on the electrodes without reaching the collector. This simulation clearly demonstrates selective filtration of ions by varying compensation voltage in DMS.

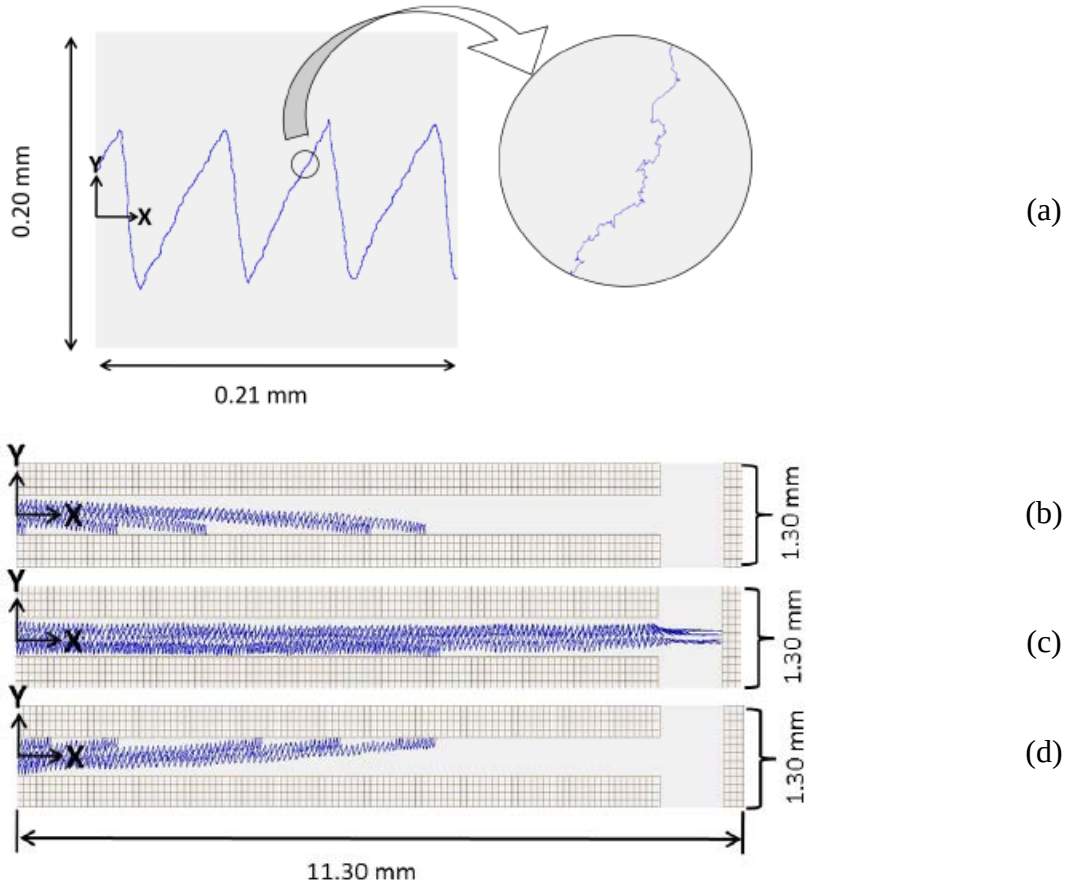

Figure 23. $H^+(H_2O)_n$ ions trajectories (a) in the DMS with 600-V RF voltage for various compensation voltages: (b) 0 V, (c) -3 V, and (d) -6 V.

DMS filtration gap dimensions are 0.5mm height and 10mm length, which are the same as the gap used in the Sionex DMS.

A.3 Membrane Permeation Simulation

Figure 24 shows two time profiles of the Cl peak measured after the membrane was place in sealed 80-ppmv TCE-water solution for two flow rates of transport gas, (a) 30 SCCM and (b) 80 SCCM. Both the experimental data and the calculated results indicate that the TCE concentration in air increases initially, reaches a peak value, and then decreases. For the higher flow rate (80 SCCM), the Cl peak intensity in later times decays faster and the maximum intensity is lower than those for 30 SCCM. The faster decay is attributed to a larger permeation rate under a higher flow rate. This correlation suggests that transport flow indeed leads to a large difference of the concentrations between the membrane layers.

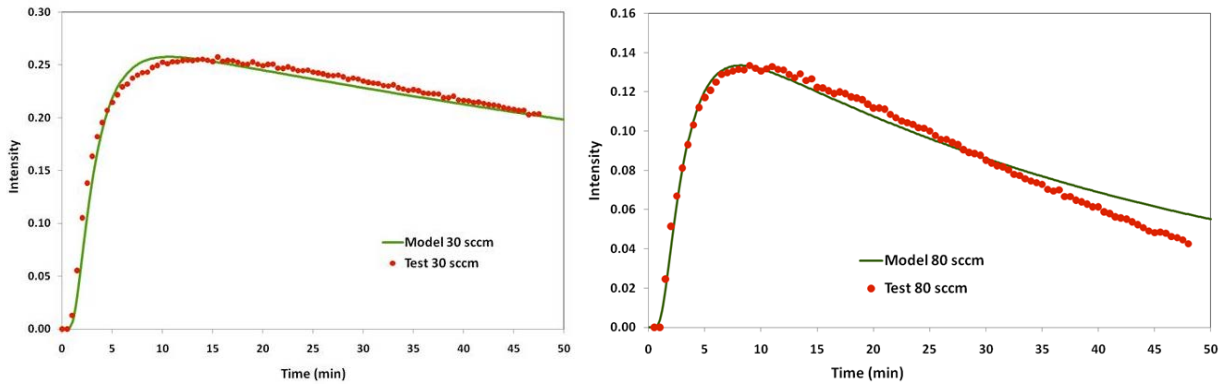

Figure 24. Comparison between the experimental data and the calculated results for an air flow rate of (a) 30 SCCM and (b) 80 SCCM.

Table 3. Calculated and fitted parameters for two flow rates.

Carrier Gas Flow	30 SCCM	80 SCCM
P	5.0×10^{-5} m s^{-1}	1.6×10^{-4} m s^{-1}
A	7.5×10^{-3} s^{-1}	7.5×10^{-3} s^{-1}
Average air velocity	0.28 m sec^{-1}	0.75 m sec^{-1}

In Figure 24, the theoretical modeling of the time profiles for the two flow rates are plotted as solid lines. In these calculations, the parameters "P" and "A" were first fitted to the experimental data for 30 SCCM. Then "A" was maintained the same for both flow rates because it mainly depends on the permeating chemical and membrane, which are the same for both flow rate measurements. A new value of "P" was obtained by fitting to the 80 SCCM experimental data. As shown in Figure 23(b), modeling with the fixed "A" is reasonably consistent with experimental data, validating the coupled fluid flow and mass transport model.

As shown in Table 3, the fitted apparent permeability increases with the air flow rate. In other words, the permeation flux of TCE through the membrane wall increases as the flow rate rises. Since it doesn't consider the details of TCE permeation, this simplified model is not able to explain the dependence of permeation flux on the flow rate. However, this trend is consistent with that reported in the literature (Banat and Simandl, 1996). In that study, benzene was removed from a gas mixture through a membrane into an aqueous solution and the benzene mass transfer flux increased with the liquid flow rate. A detailed study of TCE permeation through the membrane layer is planned in the future to verify several assumptions used here and to gain a better understanding of the process.

Figure 25 shows the distribution of normalized TCE concentration in water and air near the tube exit at two different times. The TCE concentration is normalized over the initial concentration of 80 ppm. The TCE concentration in water decreases with time as TCE permeates through the membrane layer and is carried away by the air flow. The air flow velocity varies parabolically from zero at the tube inner wall to the peak value at the tube center. The air flow picks up TCE as it flows through the membrane tube.

Although this model is relatively simple, the coupled fluid flow and mass transport model is able to provide insight into the mechanism of TCE concentration variation as a function of time in air. It is found that the rate of TCE concentration rise in air is controlled mainly by how fast TCE can diffuse through the membrane whereas the rate of concentration drop is dominated by the absolute amount of TCE diffusing through the membrane. All of these processes are expected to affect the response time of the IMS signal prior to reaching a steady state. It is important to know the time-dependent characteristics in order to understand both permeation mechanisms and technical sampling duty cycles.

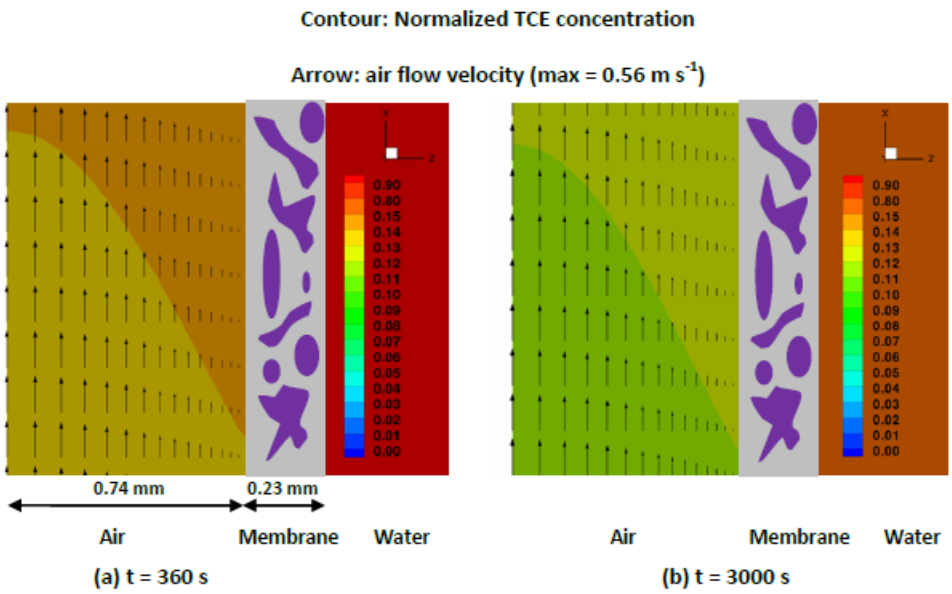

Figure 25. Modeling of the TCE concentrations distributed in water and air where color contours represent the normalized TCE concentration and arrows represent the air flow velocity.

A.4 Simulation of RF Voltage Influence

Figure 26 shows the simulated (a) and experimental (b) compensation voltage (V_C) spectra for the maximum RF voltage (V_H) varying from 500V to 900 V. At each V_H, the compensation voltage (V_C) scanned with a step of 0.5 V, the same step used in the experiment. For each V_C scan, 50 ions were inserted into the DMS entrance simultaneously. The number of the ions passing through the filtration gap was recorded automatically by a Microsoft excel file for each scan. Two phenomena were observed apparently from both the simulated and experimental results. First, the optimum V_C, defined as the V_C in which maximum number of ions passed the filtration gap, increases as V_H increases. Secondly, the efficiency of the ion transmission decreases significantly when V_H increases. The simulated results are in reasonable agreement with the experimental results.

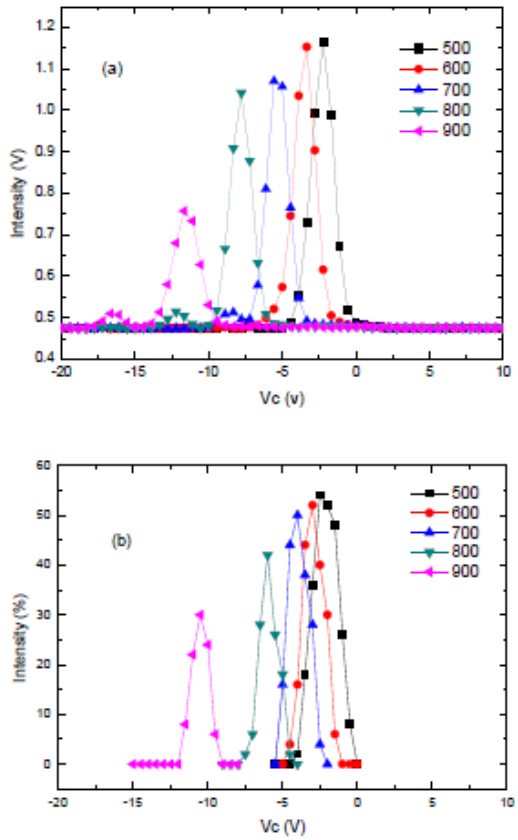

Figure 26. V_C **peak of the DMS at different V_C for the $H^+(H_2O)_n$ ion: (a) experimental; (b) calculated V_C peak.**

$M_{core\ ion}$=19, m (gas)=18, Pressure=760 torr, and Temperature=273 K.

APPENDIX B

PUBLICATIONS, PATENTS, AWARD

1. Jun Xu, Yuan Liu, International Journal of Ion Mobility Spectrometry, 2009, 12, 149-156.

2. Yongzhai Du, Wei Zhang, William Whitten, Haiyang Li, David B.Watson and J. Xu, Analytical Chemistry, 2010, 82, 4089-4096.

3. Jun Xu, Bill Whitten, and David Watson, Oak Ridge National Laboratory Special Event Award for exceeding expectation in development of groundwater monitor, 2010.

4. Wei Zhang, Yongzhai Du, Zili Feng and J. Xu, International Journal of Ion Mobility Spectrometry, 2010, 13, 65-71.

5. Jun Xu, Water Quality Products, November 2010, 15, 14-15.

6. Jun Xu, David B. Watson and William B. Whitten, Patent: Ion mobility sensor system, 2011, Pub. No.: US2011/0068264 A1

7. Jun Xu, Fenglei Han, Haiyang Li, International Journal of Ion Mobility Spectrometry, 2011, DOI 10.1007/s12127-011-0083-8

8. Yongzhai Du, David B. Watson and William B. Whitten, Erkinjon Nazarov, Haiyang Li and Jun Xu, Sensitive and Specific Sensor for Detecting Chlorinated Hydrocarbons in Water, in review.

9. Chuang Chen, Yongzhai Du, Haiyang Li and Jun Xu, Compact System for Detection of Volatile Organic Compounds in Water, in preparation.